Semiclassical theory of perpendicular transport and giant magnetoresistance in disordered metallic multilayers

Arne Brataas
Division of Physics, Faculty of Physics and Mathematics, The Norwegian Institute of Technology, University of Trondheim, 7034 Trondheim, Norway

Gerrit E. W. Bauer
Faculty of Applied Physics and Delft Institute for Microelectronics and Submicrontechnology, Delft University of Technology, Lorentzweg 1, 2628 CJ Delft, The Netherlands

(Received 1 December 1993)

The effect of disordered interfaces and bulk impurities on perpendicular transport in metallic multilayers is considered in an effective-mass semiclassical approximation. The transmission matrix is obtained by diagrammatic perturbation theory in terms of the effective-mass and conduction-band profiles at the interface. In the weak-scattering limit specular and diffuse scattering give equally important contributions to the conductance. Predictions for the transport properties of interfaces with low concentrations of strongly scattering defects should be accessible to verification by experiments. The transition from fully ballistic (Sharvin) to diffuse transport (Drude) is described analytically both in two- and three-dimensional systems, where the former case is of relevance for transport in the two-dimensional electron gas in semiconductor heterostructures. The theory is applied to the spin-valve effect in magnetic multilayers. The magnetoconductance is described by a simple formula in terms of the mean free path for the majority- and minority-spin electrons.

I. INTRODUCTION

Magnetic multilayers with a layer width down to a few Ångstrøms can be prepared by epitaxial growth techniques. Magnetic layers separated by a nonmagnetic metal layer are coupled into parallel, antiparallel, or 90° configurations, depending on the width of the spacer, the scattering properties of the bulk, and the interface roughness between the layers.[1] The coupling is similar to the oscillating indirect exchange Ruderman-Kittel-Kasuya-Yosida interaction between magnetic moments.[2] Under an applied external magnetic field, a "giant" negative magnetoresistance has been found for antiparallel multilayers.[3] The effect is caused by the reorientation of the spins under an applied external magnetic field from an antiparallel to a parallel configuration. Spin-dependent scattering at magnet/nonmagnet heterointerfaces is generally believed to be responsible for this "spin-valve" effect. Most experiments are carried out in a configuration where the current runs parallel to the interfaces [current in plane (CIP)]. The perpendicular transport configuration where the current runs perpendicular to the interfaces [current perpendicular to plane (CPP)] is attractive because of a larger magnetoresistance.[4–10] Furthermore, the theoretical description becomes more transparent due to the higher symmetry. The considerable experimental difficulties caused by the very low resistance of CPP samples have been overcome by superconducting electronics[4] or by using microstructured samples.[5] The latter solution allows the study of the perpendicular transport at higher temperatures and, at least in principle, in the mesoscopic regime.

The present paper is devoted to the theory of perpendicular transport in magnetic multilayers. The aim is to describe the effects of interface roughness scattering, bulk impurity scattering, and discontinuities in the conduction-band profile and effective masses. The importance of interface roughness scattering in many areas of metal and semiconductor physics is reflected by numerous papers since the seminal work by Fuchs,[11] e.g., in the two-dimensional electron gas.[12] The relation between diffuse and specular scattering at an interface is usually described by introducing a factor p which is determined empirically or derived from a microscopic model of the interface roughness.[11,13] Our semiclassical approach based on the Landauer-Büttiker formalism[14] gives a simple formula for the specularity parameter for transmission and reflection. The diffuse and specular contributions to the interface roughness are shown to be equally important in the weak-scattering limit.[16] The semiclassical calculation also gives analytical results for the transition from the ballistic regime (Sharvin) to the Ohmic limit (Drude) for both two-dimensional (2D) and 3D systems. Preliminary results of the present paper have been published in Refs. 15–17. The paper is organized as follows. The ballistic regime is treated in Sec. II. A theoretical description of interface roughness and bulk impurity scattering is presented in Sec. III. Approximations have to be made. In Sec. IV approximate expressions are derived for transmission through a single disordered interface which becomes exact in the weak-scattering limit. A semiclassical generalization to multilayers is given in Sec. V and applied to the spin-valve effect in magnetic multilayers. Finally, the conclusions are summarized in Sec. VI.

II. THE BALLISTIC REGIME

A model of the multilayer system is shown in Fig. 1. $N_{\rm bi}$ bilayers of normal/ferromagnetic metals are inserted between the contacts. If the contacts are in thermodynamic equilibrium, the Landauer-Büttiker formalism is suitable to describe the transport process. In the two-current model the conductance is given by

$$G = \frac{e^2}{h} \sum_{nm,s} |t_{nm,s}|^2, \tag{1}$$

where $t_{nm,s}$ is the transmission amplitude from mode m to mode n for electrons with spin s. Inelastic scattering and spin-flip processes are disregarded, since at low temperature the spin-flip relaxation length due to spin-orbit effects and by scattering by magnetic impurities is normally much larger than the mean free path. Spin-flip scattering due to excited magnons becomes important at higher temperatures, where the present theory is not valid anymore.

Even mesoscopic sample dimensions of ~ 1 μm are much larger than the typical Fermi wavelength (~ 5 Å). The incoming and outgoing states may therefore be modeled by Bloch waves, which will be approximated by plane waves.[7] For magnetic multilayers our model corresponds to the Stoner description of itinerant ferromagnetism.[18] In the ferromagnetic metal, the density is different for majority and minority spins, which leads to a spin-dependent shift of the band edges when the Fermi energies align. Band structure and electron-density effects are included by means of a constant, metal- and spin-dependent potential and an isotropic effective mass for each spin in each layer. The ballistic regime will be treated first.[7] Semiclassically, the Sharvin conductance in a 3D point contact is[19]

$$G_0 = \frac{2e^2}{h} \frac{k_F^2 A}{4\pi}, \tag{2}$$

where k_F is the Fermi wave vector and A is the sample cross section. For an ideal multilayer structure, the total conductance is equal to the contact conductance. If treated semiclassically, the conductance is

$$G_{\rm con} = G_0 \left[1 - \frac{\max\{0, \Delta \mathrm{U}\}}{\mathrm{E_F}} \right], \tag{3}$$

where ΔU is the conduction-band shift. This result is a good approximation to the fully quantum mechanical expressions.[8] The conduction-band shift, as seen by the majority and minority spins in the parallel and antiparallel configurations, are shown in Fig. 2. For the antiparallel configuration, the conduction-band profile has the same form for the majority spin and the minority spin. The transmission probabilities for the majority- and minority-spin electrons are different for the parallel configuration. The conductance is therefore larger in the parallel configuration than in the antiparallel configuration. The result for the magnetoconductance, $\Delta G_{\rm con} = G^P_{\rm con} - G^{AP}_{\rm con}$, can be found by using Eq. (3) for the parallel and the antiparallel case. The magnetoconductance is

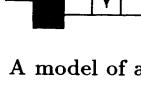

FIG. 1. A model of a magnetic multilayer structure.

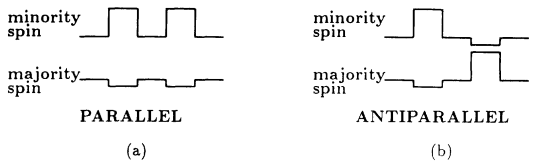

FIG. 2. The conduction-band profile as seen by the minority-spin electrons and the majority-spin electrons in the parallel and the antiparallel configurations.

$$\frac{\Delta G_{\rm con}}{G_0} = \frac{\max\{0, \Delta \mathrm{U_{min}}\} - \max\{0, \Delta \mathrm{U_{maj}}\}}{2\mathrm{E_F}}, \tag{4}$$

where $\Delta U_{\rm maj}$ ($\Delta U_{\rm min}$) is the conduction-band shift for majority (minority) spins in the ferromagnetic material. In the semiclassical approximation only the first bilayer contributes to the conductance, so the magnetoconductance is independent of the number of layers. In this model a sizable effect may be expected for the Cu/Co system: The electronic structure of the Co majority-spin system is similar to that of copper, causing a small $\Delta U_{\rm maj}$, while the density of the minority-spin electrons is smaller, i.e., $\Delta U_{\rm min} > 0$. Using the parameters of Inoue, Oguri, and Maekawa[20] for the Co/Cu system ($\Delta U_{\rm min} \approx 0.65$ eV, $\Delta U_{\rm maj} \approx 0$ eV) and assuming that transport is carried mainly by s electrons ($E_F \approx 9.4$ eV), $\Delta G_{\rm con}/G_0 \approx 0.04$ is obtained. It is clear that this simple theory cannot explain the large experimental magnetoconductances, especially in materials such as the Cr/Fe system where the shift in the conduction band is negative and Eq. (4) vanishes.

A semiclassical approximation has been made. It is possible to calculate the transmission probabilities exactly for a Kronig-Penney potential.[21] Although quantum effects partly average out in the sum over different modes contributing to the total conductance, in a tight-binding approximation significant effects have been predicted for thin layers with relatively large potential steps.[10] Whether or not a step in the conduction-band profile can explain the giant magnetoresistance also depends on the detailed band structure.[17] In the next sections, spin-dependent scattering due to interface roughness or bulk impurities will be included, which is seen to enhance the magnetoconductance.

III. INTERFACE ROUGHNESS AND IMPURITY SCATTERING

Interface roughness is due to lattice mismatch or lattice defects that destroy the periodicity. The interface is not perfectly sharp, so that the different materials will

be mixed at an interface sheet. The effect of interface scattering will be modeled by short-range scatterers in a plane, which can be motivated by the strong screening in high-density metals. These results will be generalized to treat bulk impurity scattering and interdiffused interfaces. The impurity positions are not known. The transmission properties of present interest are therefore the average over all relevant ensembles. The transmission process may be visualized by Feynman diagrams. In order to obtain closed formulas, approximations will be made by only including diagrams that are most important in terms of a scattering parameter.

A. Scattering by δ potentials in a plane

In the effective-mass approximation, scattering of electrons by short-range scattering centers can be treated exactly.[21,22] The single-electron state is described by the Schrödinger equation

$$\left(-\frac{\hbar^2}{2}\nabla\frac{1}{m^*(x)}\nabla + U_C(x) + V(x,y,z)\right)\psi(x,y,z) = E\psi(x,y,z), \quad (5)$$

with an arbitrary conduction-band profile $U_C(x)$. The effective mass $m^*(x)$ may be metal and spin dependent. Interface roughness gives rise to the scattering potential $V(x,y,z)$. The wave function can be expanded in the complete set of eigenstates,

$$\psi(x,\vec{\rho}) = \sum_{\vec{k}_\parallel} c_{\vec{k}_\parallel}(x)\phi_{\vec{k}_\parallel}(\vec{\rho}), \quad (6)$$

where $\vec{\rho} = (y,z)$. The transverse parts of the wave function are plane waves given by

$$\phi_{\vec{k}_\parallel}(\vec{\rho}) = \frac{e^{i\vec{k}_\parallel\vec{\rho}}}{\sqrt{A}}, \quad (7)$$

where A is the area of the interface. In this way, the transverse wave functions are normalized to unity in the transverse directions. Impurity scattering gives rise to mixing between different transverse modes. Using the orthogonality of the transverse wave functions, a one-dimensional equation can be obtained for the longitudinal wave functions,

$$m^*(x)\left(\frac{d}{dx}\right)\frac{1}{m^*(x)}\left(\frac{d}{dx}\right)c_{\vec{k}_\parallel}(x) + k_\perp^2(x)c_{\vec{k}_\parallel}(x) = \sum_{\vec{k}'_\parallel} V_{\vec{k}_\parallel,\vec{k}'_\parallel}(x)c_{\vec{k}'_\parallel}(x), \quad (8)$$

where the perpendicular wave vector is

$$k_\perp^2(x) = \frac{2m^*(x)}{\hbar^2}[E - U_C(x)] - k_\parallel^2, \quad (9)$$

and the scattering coefficients $V_{\vec{k}_\parallel,\vec{k}'_\parallel}$ are defined by

$$V_{\vec{k}_\parallel,\vec{k}'_\parallel}(x) \equiv \frac{2m^*(x)}{\hbar^2}\int d\vec{\rho}\,\phi^*_{\vec{k}_\parallel}(\vec{\rho})V(x,y,z)\phi_{\vec{k}'_\parallel}(\vec{\rho}). \quad (10)$$

The conduction-band profile is a Kronig-Penney potential for magnetic multilayers. Now we consider only a single interface. The conduction-band profile and the effective mass are then step functions at the interface:

$$U_C(x) = \begin{cases} U_L & x < 0 \\ U_R & x > 0 \end{cases} \quad (11)$$

and

$$m^*(x) = \begin{cases} m_L^* & x < 0 \\ m_R^* & x > 0. \end{cases} \quad (12)$$

For simplicity, the scattering potentials are modeled by δ-impurity scatterers

$$V(x,y,z) = \sum_\alpha \gamma_\alpha \delta(x)\delta(\vec{\rho} - \vec{\rho}_\alpha), \quad (13)$$

where $\vec{\rho}_\alpha$ gives the transverse position of the scattering center, and γ_α gives the strength of the scatterer. It will be shown below that a zero-range potential leads to divergences, which means that the δ functions should represent hard spheres with small but finite diameter. If all disorder is at the interface, the strength of the scatterers can be simply estimated by $|\gamma_\alpha| \approx ((|U_R - U_L|)/2)(a/2)^3$, where a is the lattice constant. Inserting the scattering potential Eq. (13) into Eq. (8), the one-dimensional equation can be written as

$$\left(\frac{d}{dx}\right)\frac{1}{m^*(x)}\left(\frac{d}{dx}\right)c_{\vec{k}_\parallel}(x) + \frac{k_\perp^2(x)}{m^*(x)}c_{\vec{k}_\parallel}(x) = \sum_{\vec{k}'_\parallel}\frac{\tilde{\Gamma}_{\vec{k}_\parallel,\vec{k}'_\parallel}}{\bar{m}^*}\delta(x)c_{\vec{k}'_\parallel}(x), \quad (14)$$

where an averaged effective mass, $\bar{m}^* \equiv \sqrt{m_R^* m_L^*}$, is defined. The transverse part of the δ function is integrated out, and a scattering matrix is defined,

$$\tilde{\Gamma}_{\vec{k}_\parallel,\vec{k}'_\parallel} \equiv \sum_\alpha \frac{2\bar{m}^*\gamma_\alpha}{\hbar^2}\phi^*_{\vec{k}_\parallel}(\vec{\rho}_\alpha)\phi_{\vec{k}'_\parallel}(\vec{\rho}_\alpha). \quad (15)$$

Integrating across the $\delta(x)$ function we get

$$\frac{\sqrt{m_L^* m_R^*}}{m_R^*}\frac{dc_{\vec{k}_\parallel}(x)}{dx}\bigg|_{x=0^+} - \frac{\sqrt{m_R^* m_L^*}}{m_L^*}\frac{dc_{\vec{k}_\parallel}(x)}{dx}\bigg|_{x=0^-} = \sum_{\vec{k}'_\parallel}\tilde{\Gamma}_{\vec{k}_\parallel,\vec{k}'_\parallel}c_{\vec{k}'_\parallel}(0). \quad (16)$$

We assume that the particles are incident with parallel momentum $\vec{k}'_\parallel$. The incoming wave gives rise to an infinite set of modes, propagating for real $k'_\perp$, and evanescent for imaginary $k'_\perp$. The transmission (reflection) matrix is $t_{\vec{k}_\parallel,\vec{k}'_\parallel}$ ($r_{\vec{k}_\parallel,\vec{k}'_\parallel}$). The conductance is given by the summation over all propagating modes in both indices. The

wave function is

$$c_{\vec{k}_\parallel}(x) = \begin{cases} \sqrt{\frac{m_L^*}{\hbar|k_\perp^L|}}\delta_{\vec{k}_\parallel,\vec{k}'_\parallel} e^{ik_\perp^L x} + \sqrt{\frac{m_L^*}{\hbar|k_\perp^L|}} r_{\vec{k}_\parallel,\vec{k}'_\parallel} e^{-ik_\perp^L x}, & x<0 \\ \sqrt{\frac{m_R^*}{\hbar|k_\perp^R|}} t_{\vec{k}_\parallel,\vec{k}'_\parallel} e^{ik_\perp^R x}, & x>0 \end{cases} \tag{17}$$

for propagating and evanescent states, where evanescent states are exponentially localized at the interface. The longitudinal parts of the wave function $c_{\vec{k}_\parallel}(x)$ are normalized to carry unit flux. The continuity relation for the wave function is

$$r_{\vec{k}_\parallel,\vec{k}'_\parallel} = \sqrt{\frac{m_R^*|k_\perp^L|}{m_L^*|k_\perp^R|}} t_{\vec{k}_\parallel,\vec{k}'_\parallel} - \delta_{\vec{k}_\parallel,\vec{k}'_\parallel}. \tag{18}$$

The maximum transverse wave vectors corresponding to propagating modes are

$$k_{\parallel,\max}^R = \sqrt{\frac{2m_R^*}{\hbar^2}(E-U^R)} \tag{19}$$

to the right of the interface and

$$k_{\parallel,\max}^L = \sqrt{\frac{2m_L^*}{\hbar^2}(E-U^L)} \tag{20}$$

to the left of the interface. In the following, we assume that $k_{\parallel,\max}^R \geq k_{\parallel,\max}^L$. (The results are similar for $k_{\parallel,\max}^R \leq k_{\parallel,\max}^L$.) Current conservation dictates that

$$\sum_{\vec{k}_\parallel}^{|\vec{k}_\parallel|\leq k_{\parallel,\max}^R} T_{\vec{k}_\parallel,\vec{k}'_\parallel} + \sum_{\vec{k}_\parallel}^{|\vec{k}_\parallel|\leq k_{\parallel,\max}^L} R_{\vec{k}_\parallel,\vec{k}'_\parallel} = 1, \tag{21}$$

where the summations are only over propagating modes. The continuity relation for the wave function and current conservation give a relation between the transmission probabilities, $T_{\vec{k}_\parallel,\vec{k}'_\parallel} = |t_{\vec{k}_\parallel,\vec{k}'_\parallel}|^2$, and the transmission coefficients $t_{\vec{k}_\parallel,\vec{k}'_\parallel}$,

$$\sum_{\vec{k}_\parallel}^{|\vec{k}_\parallel|\leq k_{\parallel,\max}^L} \frac{\bar{k}_\perp}{k_\perp^R} T_{\vec{k}_\parallel,\vec{k}'_\parallel} + \frac{1}{2}\sqrt{\frac{m_L^*}{m_R^*}} \sum_{|\vec{k}_\parallel|\geq k_{\parallel,\max}^L}^{|\vec{k}_\parallel|\leq k_{\parallel,\max}^R} T_{\vec{k}_\parallel,\vec{k}'_\parallel} = \sqrt{\frac{k'^L_\perp}{k'^R_\perp}}\,\mathrm{Re}(t_{\vec{k}'_\parallel,\vec{k}'_\parallel}), \tag{22}$$

where an intermediate perpendicular wave vector is introduced as

$$\bar{k}_\perp \equiv \frac{m_R^* k_\perp^L + m_L^* k_\perp^R}{2\sqrt{m_L^* m_R^*}}. \tag{23}$$

This identity can be considered as a special case of the optical theorem.[23] In the symmetric case, the relation $\sum_{\vec{k}_\parallel} T_{\vec{k}_\parallel,\vec{k}'_\parallel} = \mathrm{Re}(t_{\vec{k}'_\parallel,\vec{k}'_\parallel})$ holds. These identities will be used to check if our approximations are consistent and in a semiclassical approximation it relates specular and diffuse scattering for perpendicular transport through an interface. It will also drastically simplify semiclassical calculations of the multilayer conductance. Green functions are introduced in the next subsection, where it is shown that Eq. (22) relates two-particle Green functions to a single-particle Green function.

Combining Eqs. (16), (17), and (18), we find that the transmission coefficients are solutions to the equation

$$\sum_{\vec{k}''_\parallel}[\delta_{\vec{k}_\parallel,\vec{k}''_\parallel} + i\tilde{\Gamma}_{\vec{k}_\parallel,\vec{k}''_\parallel}\sqrt{\frac{|k_\perp^R|}{|k''^R_\perp|}}\frac{1}{2\bar{k}_\perp}]t_{\vec{k}''_\parallel,\vec{k}'_\parallel} = \frac{\sqrt{|k_\perp^L||k_\perp^R|}}{\bar{k}_\perp}\delta_{\vec{k}_\parallel,\vec{k}'_\parallel}. \tag{24}$$

This can be written in matrix notation as (a matrix is indicated by double bars) $(\bar{\bar{I}} + i\bar{\bar{\Gamma}})\cdot\bar{\bar{t}} = \bar{\bar{\Lambda}}$, where

$$\Lambda_{\vec{k}_\parallel,\vec{k}'_\parallel} \equiv \delta_{\vec{k}_\parallel,\vec{k}'_\parallel}\frac{\sqrt{|k_\perp^L||k_\perp^R|}}{\bar{k}_\perp} \tag{25}$$

and

$$\Gamma_{\vec{k}_\parallel,\vec{k}'_\parallel} \equiv \sum_\alpha \frac{\bar{m}^*\gamma_\alpha}{A\hbar^2}\frac{\sqrt{|k_\perp^R|}}{\bar{k}_\perp} e^{-i\vec{k}_\parallel\vec{\rho}_\alpha}\frac{1}{\sqrt{|k'^R_\perp|}} e^{i\vec{k}'_\parallel\vec{\rho}_\alpha}. \tag{26}$$

Expanding in a power series in $\bar{\bar{\Gamma}}$ we obtain

$$\bar{\bar{t}} = \sum_{N=0}^{\infty}(-i\bar{\bar{\Gamma}})^N\bar{\bar{\Lambda}}. \tag{27}$$

The transmission coefficient is given as a series expansion in the scattering matrix.

By Eqs. (24)–(27) the transmission coefficients are now, in principle, known. However, the impurities are randomly located. It is not trivial to find the configurational average. Physical motivated arguments have to be found. Green functions are introduced in the next subsection in order to understand the physical processes.

B. Green functions

The series expansion can be visualized using standard diagrammatic techniques. A subset of all diagrams can then be summed to approximate the transmission probability. In this subsection the relation between transmission coefficients and Green functions will be explained.[24–26] Although the procedure is well known in principle,[27] to the best of our knowledge a thorough discussion in the context of the Landauer-Büttiker formalism does not exist.

The Green operator is defined as $G^{\pm} = (E - H \pm i\eta)^{-1}$ where η is a positive infinitesimal. At low temperature, the transport is governed by the electrons at the Fermi level. The energy E of the Green function will henceforth be taken to be E_F and will be suppressed. In coordinate space, the Green function is $G^{\pm}(\vec{r},\vec{r'}) = \langle\vec{r}|G^{\pm}|\vec{r'}\rangle$. In our problem, the interesting Green function is the one where propagation from left to right is considered. This Green function can be expanded in the set of eigenstates on both sides of the interface,

$$G^{+}(\vec{r}_R,\vec{r}_L) = \sum_{\vec{k}_{\parallel},\vec{k}'_{\parallel}} G^{+}_{\vec{k}_{\parallel},\vec{k}'_{\parallel}} e^{ik^R_{\perp}x_R} e^{i\vec{k}_{\parallel}\vec{\rho}_R} \times e^{-ik'^L_{\perp}x_L} e^{-i\vec{k}'_{\parallel}\vec{\rho}_L}, \tag{28}$$

where $\vec{r}_{R,L} = (x_{R,L}, \vec{\rho}_{R,L})$ and $x_R > 0$, $x_L < 0$. The summation includes both propagating and evanescent states. $G^{+}_{\vec{k}_{\parallel},\vec{k}'_{\parallel}}$ is related to the transmission matrix by[24–26]

$$t_{\vec{k}_{\parallel},\vec{k}'_{\parallel}} = i\hbar^2\sqrt{\frac{|k^R_{\perp}||k'^L_{\perp}|}{m^*_R m^*_L}}\, G^{+}_{\vec{k}_{\parallel},\vec{k}'_{\parallel}}. \tag{29}$$

The (diagonal) unperturbed Green function is

$$G^{+(0)}_{\vec{k}_{\parallel}} = -i\frac{\bar{m}^*}{\hbar^2}\frac{1}{\bar{k}_{\perp}}. \tag{30}$$

Note that following Refs. 24–26, the dimension of $G_{\vec{k}_{\parallel},\vec{k}'_{\parallel}}$ is $[Jm]^{-1}$ and not $[J]^{-1}$ as for conventional Green functions. The series expansion for the transmission coefficients will now give a similar expansion for the Green function. The relation between the transmission coefficients and the transmission probabilities, Eq. (22), gives for the Green function

$$\sum_{\vec{k}_{\parallel}}^{|\vec{k}_{\parallel}|\le k^L_{\parallel,\max}} \frac{|G^{+}_{\vec{k}_{\parallel},\vec{k}'_{\parallel}}|^2}{G^{+(0)}_{\vec{k}_{\parallel}}} + \frac{1}{2}\sqrt{\frac{m^*_L}{m^*_R}} \sum_{|\vec{k}_{\parallel}|\ge k^L_{\parallel,\max}}^{|\vec{k}_{\parallel}|\le k^R_{\parallel,\max}} \frac{k^R_{\perp}}{k^L_{\perp}} \frac{|G^{+}_{\vec{k}_{\parallel},\vec{k}'_{\parallel}}|^2}{G^{+(0)}_{\vec{k}_{\parallel}}} = -i\mathrm{Im}(G^{+}_{\vec{k}'_{\parallel},\vec{k}'_{\parallel}}). \tag{31}$$

This is a relation between two-particle (particle-hole) Green functions and a single-particle Green function. We will show that this identity gives the connection between the self-energy and the vertex function for the particle-hole propagator.

The evaluation of the configurational average of the series for the Green functions is considered in the next subsection, where the different diagrams are shown, and the Feynman rules are outlined.

C. Feynman diagrams

The positions of the impurity scatterers are not known in a real material. The transmission probabilities of present interest are, therefore, the ensemble average of all possible configurations for the impurities. The configurational average of a quantity is the average over all impurity positions,

$$\langle\theta(\vec{\rho}_1,\ldots,\vec{\rho}_N)\rangle \equiv \prod_{\alpha=1}^{N}\int\frac{d\vec{\rho}_{\alpha}}{A}\theta(\vec{\rho}_1,\ldots,\vec{\rho}_N). \tag{32}$$

The Green functions can be organized into a diagrammatic visualization using Feynman diagrams. We will now explain the relation between the algebraic and the diagrammatic representation of the Green function. In Sec. III A it was shown that the transmission coefficient could be expressed as a series expansion in the scattering matrix $\bar{\bar{\Gamma}}$. The electron Green function is related to the transmission coefficient by a normalization factor. From Eqs. (27) and (29), the electron Green function reads

$$\langle G^{+}_{\vec{k}_{\parallel},\vec{k}'_{\parallel}}\rangle = -i\frac{\bar{m}^*}{\hbar^2}\frac{1}{\sqrt{|k^R_{\perp}||k'^L_{\perp}|}} \times\sum_{N=0}^{\infty}\langle(-i\bar{\bar{\Gamma}})^N\rangle_{\vec{k}_{\parallel},\vec{k}'_{\parallel}}\frac{\sqrt{|k'^L_{\perp}||k'^R_{\perp}|}}{\bar{k}'_{\perp}}. \tag{33}$$

Similarly, the electron-hole Green function is

$$\langle G^{+}_{\vec{k}_{\parallel},\vec{k}'_{\parallel}} G^{+(*)}_{\vec{k}_{\parallel},\vec{k}'_{\parallel}}\rangle = |-i\frac{\bar{m}^*}{\hbar^2}|^2\frac{1}{|k^R_{\perp}||k'^L_{\perp}|}\left\langle\left\{\sum_{N=0}^{\infty}(-i\bar{\bar{\Gamma}})^N\right\}_{\vec{k}_{\parallel},\vec{k}'_{\parallel}}\left\{\sum_{M=0}^{\infty}(i\bar{\bar{\Gamma}}^*)^M\right\}_{\vec{k}_{\parallel},\vec{k}'_{\parallel}}\right\rangle\frac{|k'^L_{\perp}||k'^R_{\perp}|}{(\bar{k}'_{\perp})^2}. \tag{34}$$

In order to evaluate these expressions the ensemble average $\langle(-i\bar{\bar{\Gamma}})^N(i\bar{\bar{\Gamma}}^*)^M\rangle$ has to be known for all N and M. We will now show for the first three terms that the series expansion of the electron Green function can be expressed as a series in the unperturbed Green function and scattering vertices. The zeroth order term gives

$$-i\frac{\bar{m}^*}{\hbar^2}\frac{1}{\sqrt{|k^R_{\perp}||k'^L_{\perp}|}}\langle(-i\bar{\bar{\Gamma}})^0\rangle_{\vec{k}_{\parallel},\vec{k}'_{\parallel}}\frac{\sqrt{|k'^L_{\perp}||k'^R_{\perp}|}}{\bar{k}'_{\perp}} = -i\frac{\bar{m}^*}{\hbar^2}\frac{1}{\bar{k}_{\perp}}\delta_{\vec{k}_{\parallel},\vec{k}'_{\parallel}} = G^{+(0)}_{\vec{k}_{\parallel}}\delta_{\vec{k}_{\parallel},\vec{k}'_{\parallel}}, \tag{35}$$

which is simply the unperturbed diagonal Green function. Without scattering, only this term survives. For the next term in the series, we find

$$-i\frac{\bar{m}^*}{\hbar^2}\frac{1}{\sqrt{|k_\perp^R||k'^L_\perp|}}\langle(-i\bar{\bar{\Gamma}})^1\rangle_{\vec{k}_\parallel,\vec{k}'_\parallel}\frac{\sqrt{|k'^L_\perp||k'^R_\perp|}}{\bar{k}'_\perp}=\left(-i\frac{\bar{m}^*}{\hbar^2}\frac{1}{\bar{k}_\perp}\right)\left(\frac{1}{A}\sum_\alpha\gamma_\alpha\right)\left(-i\frac{\bar{m}^*}{\hbar^2}\frac{1}{\bar{k}_\perp}\right)\delta_{\vec{k}_\parallel,\vec{k}'_\parallel}$$

$$=G^{+(0)}_{\vec{k}_\parallel}\left(\frac{1}{A}\sum_\alpha\gamma_\alpha\right)G^{+(0)}_{\vec{k}_\parallel}\delta_{\vec{k}_\parallel,\vec{k}'_\parallel}. \tag{36}$$

This is a description of a single scattering by a single impurity. The third and last term we discuss is

$$-i\frac{\bar{m}^*}{\hbar^2}\frac{1}{\sqrt{|k_\perp^R||k'^L_\perp|}}\langle(-i\bar{\bar{\Gamma}})^2\rangle_{\vec{k}_\parallel,\vec{k}'_\parallel}\frac{\sqrt{|k'^L_\perp||k'^R_\perp|}}{\bar{k}'_\perp}=-i\frac{\bar{m}^*}{\hbar^2}\frac{1}{\sqrt{\bar{k}_\perp\bar{k}'_\perp}}[\langle(-i\bar{\bar{\Gamma}})^1\rangle_{\vec{k}_\parallel,\vec{k}'_\parallel}]^2-\delta_{\vec{k}_\parallel,\vec{k}'_\parallel}N_{IR}\left(\frac{1}{A}\frac{\bar{m}^*\gamma}{\hbar^2}\right)^2\frac{1}{\bar{k}_\perp}\sum_{\vec{k}''_\parallel}\frac{1}{\bar{k}''_\perp}$$

$$=G^{+(0)}_{\vec{k}_\parallel}\left(\frac{1}{A}\sum_\alpha\gamma_\alpha\right)G^{+(0)}_{\vec{k}_\parallel}\left(\frac{1}{A}\sum_\alpha\gamma_\alpha\right)G^{+(0)}_{\vec{k}_\parallel}\delta_{\vec{k}_\parallel,\vec{k}'_\parallel}$$

$$+G^{+(0)}_{\vec{k}_\parallel}\left(\sum_\alpha(\frac{\gamma_\alpha}{A})^2\right)\sum_{\vec{k}''_\parallel}(G^{+(0)}_{\vec{k}''_\parallel})G^{+(0)}_{\vec{k}_\parallel}\delta_{\vec{k}_\parallel,\vec{k}'_\parallel} \tag{37}$$

where N_{IR} is the number of impurities. Now there are two possibilities. The electron can be scattered by two different scatterers once or by a single scatterer twice.

Each factor $\Gamma_{\vec{k}_\parallel,\vec{k}'_\parallel}$ describes a single scattering process. For higher order terms, the electron may scatter several times with the same impurity. These terms can be represented by Feynman diagrams, where the cross represents an impurity, the dashed line represents scattering, and the plain line represent free electron or hole propagation. Electrons propagate forward in time, from the left to the right and holes in the opposite direction. The first three terms in the electron Green function, Eq. (35), Eq. (36), and Eq. (37) are shown in Fig. 3. The first diagram (a) is simply the unperturbed single-electron Green function. Diagrams of types (b), (c), and (d) modify separately the propagation of electrons. The complex conjugate of these terms will give diagrams that modify the propagation of holes.

Similarly, we get an expansion series for the electron-hole propagator. This series should include the correlation between the scattering potential seen by electrons and holes. The first terms in the series expansion of the electron-hole Green functions are shown in Fig. 4. Diagram (a) describes a scattering without correlation. Diagrams of type (b) describe the correlated scattering of electrons and holes. It turns out that these diagrams describe diffuse scattering at the interface.

On averaging over random positions of impurities, one

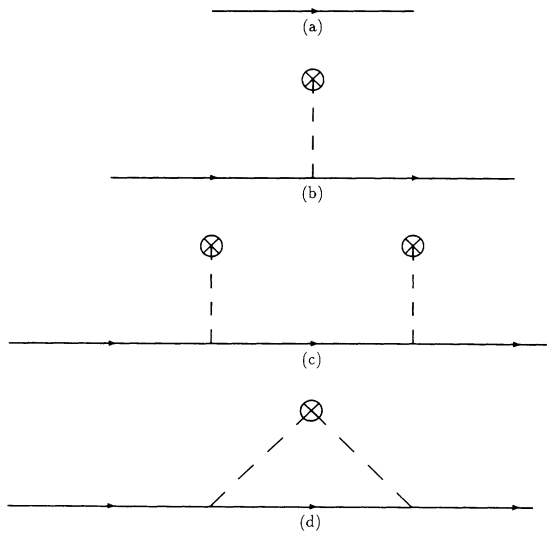

FIG. 3. Diagrams for the single-electron propagator.

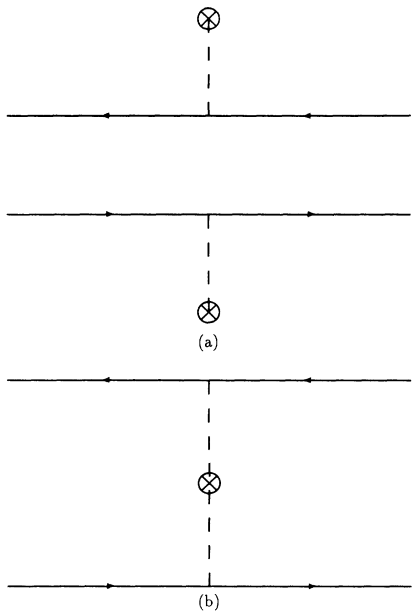

FIG. 4. Diagrams for the electron-hole propagator.

finds that electron momentum is conserved. When evaluating the different diagrams, the following Feynman rules can be found by inspection of the ensemble average.

(1) For each electron line, introduce $-i\bar{m}^*/\hbar^2\bar{k}_\perp$.

(2) For each hole line, introduce $i\bar{m}^*/\hbar^2\bar{k}_\perp$.

(3) For each scattering vertex, introduce (γ_α/A) where α labels the scattering center.

(4) Momentum conservation at each vertex.

(5) Sum over all impurities, $\sum_\alpha$.

(6) Sum over all intermediate states.

The single propagator is a sum over all kinds of diagrams that describe impurity scattering. These can be partially summed by introducing the irreducible self-energy. An irreducible diagram is defined as a diagram that cannot be divided into two subdiagrams joined only by a single electron or hole line. All other diagrams are called reducible. The self-energy has units $[Jm]$ in our problem because of the chosen normalization factor as discussed in Sec. III B. The single propagator can be written in terms of the self-energy by using the Dyson equation, Fig. 5. In terms of the self-energy and the unperturbed Green function, the single-particle Green function is, in matrix notation,

$$\langle\bar{\bar{G}}^+\rangle = \bar{\bar{G}}^{+(0)} + \bar{\bar{G}}^{+(0)}\bar{\bar{\Sigma}}\langle\bar{\bar{G}}^+\rangle, \tag{38}$$

where $\bar{\bar{\Sigma}}$ is the configurationally averaged irreducible self-energy. The lowest order terms in the irreducible self-energy are shown in Fig. 6.

The electron-hole Green function consists of both single diagrams for electrons and holes and correlation diagrams between electrons and holes. The uncorrelated term is simply the squared amplitude of the single electron Green function. The two-particle Green function can be written as

$$\langle|G^+_{\vec{k}_\parallel,\vec{k}'_\parallel}|^2\rangle = |\langle G^+_{\vec{k}_\parallel,\vec{k}'_\parallel}\rangle|^2 + \sum_{\vec{k}''_\parallel,\vec{k}'''_\parallel} |\langle G^+_{\vec{k}_\parallel,\vec{k}''_\parallel}\rangle|^2 W_{\vec{k}''_\parallel,\vec{k}'''_\parallel} |\langle G^+_{\vec{k}'''_\parallel,\vec{k}'_\parallel}\rangle|^2, \tag{39}$$

where $W_{\vec{k}_\parallel,\vec{k}'_\parallel}$ is the reducible vertex function. This function describes the correlation between electrons and holes and is given by the Bethe-Salpeter integral equation

$$W_{\vec{k}_\parallel,\vec{k}'_\parallel} = \sigma_{\vec{k}_\parallel,\vec{k}'_\parallel} + \sum_{\vec{k}''_\parallel,\vec{k}'''_\parallel} \sigma_{\vec{k}_\parallel,\vec{k}''_\parallel} |\langle G^+_{\vec{k}''_\parallel,\vec{k}'''_\parallel}\rangle|^2 W_{\vec{k}'''_\parallel,\vec{k}'_\parallel}, \tag{40}$$

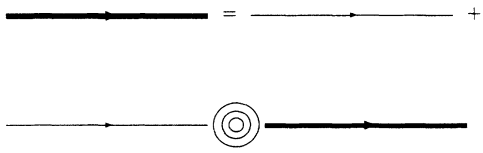

FIG. 5. The electron Green function is given in terms of the unperturbed Green function and the irreducible self-energy in the Feynman-Dyson expansion.

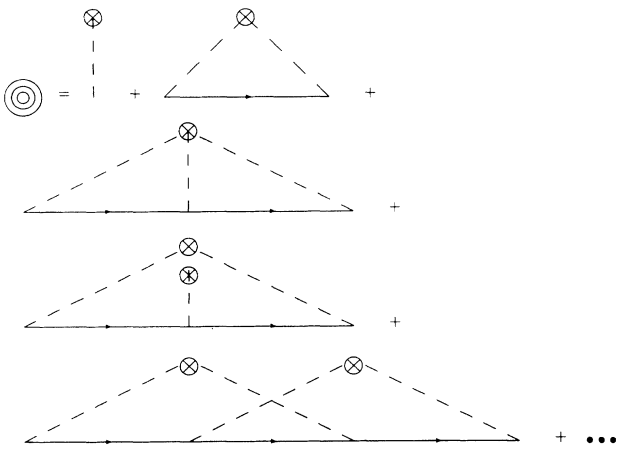

FIG. 6. The irreducible self-energy consists of all irreducible diagrams.

where $\sigma_{\vec{k}_\parallel,\vec{k}'_\parallel}$ is the irreducible vertex function (Fig. 7). The irreducible vertex function consists of all irreducible correlation terms between electrons and holes (Fig. 8). It has terms with and without crossed interaction lines. For all diagrams that are not crossed, a particular simple form of the Bethe-Salpeter integral equation can be obtained. The correlation terms between electrons and holes are referred to as vertex corrections.

In order to find the transmission probability, the self-energy has to be calculated and the Bethe-Salpeter integral equation has to be solved. In the following section this is done.

IV. SINGLE INTERFACE TRANSMISSION

The probability for transmission through a single interface will be found by using the perturbation theory described in the last section. Electrons are scattered

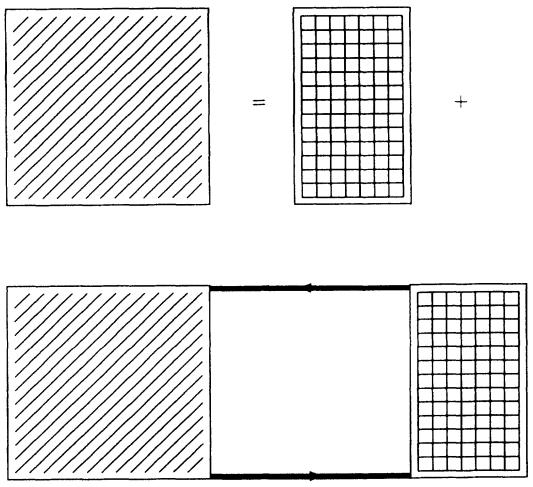

FIG. 7. The Bethe-Salpeter integral equation is a relation between the reducible and irreducible vertex functions.

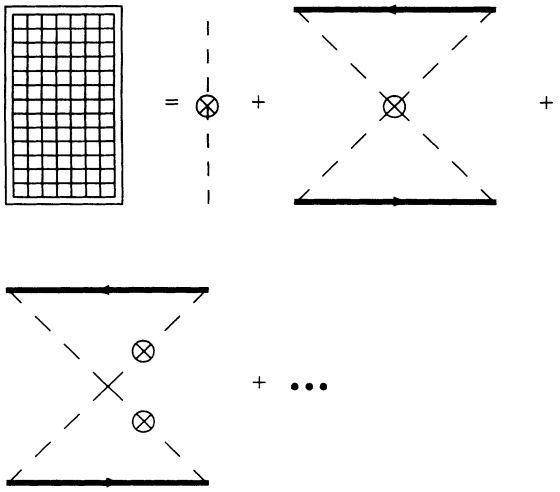

FIG. 8. The irreducible vertex function consists of all irreducible correlation diagrams between electrons and holes.

specularly at the interface if the parallel wave vector is conserved. Diffuse scattering causes a redistribution of transverse and longitudinal momentum at the interface. This nomenclature is a straightforward generalization of the diffuse vs specular reflection at impenetrable rough interfaces as introduced by Fuchs.[11] Specular and diffuse scattering for perpendicular transmission through a single interface is shown in Fig. 9.

The vertex function gives the correlation between electrons and holes. We will show that the diffuse scattering is uniquely connected to the vertex function. The optical theorem, Eq. (31), is actually a relation between specular and diffuse scattering. In order to find the two-particle Green function, the self-energy has to be calculated. We will show that the reducible vertex function can be found from the self-energy by using a semiclassical approximation. It is therefore not necessary to solve the Bethe-Salpeter integral equation directly. The self-energy is calculated in the following subsection.

A. Irreducible self-energy

The irreducible self-energy determines the single-electron propagator. In Fig. 3 a diagrammatic representation of the self-energy is shown. Conservation of momentum simplifies the calculations of the diagrams.

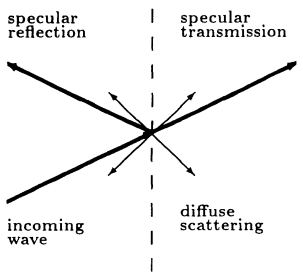

FIG. 9. Specular and diffuse scattering at a single interface.

First, translational symmetry requires that the ensemble averaged self-energy is diagonal. Second, the short-range nature of the impurity potential gives a "white" Fourier spectrum. The different terms in the self-energy will therefore only consist of summations of unperturbed Green functions times a factor. The self-energy is therefore not only diagonal, but also independent of the incoming and outgoing states, which represents a major simplification, $\Sigma_{\vec{k}_\parallel,\vec{k}'_\parallel} = \Sigma\delta_{\vec{k}_\parallel,\vec{k}'_\parallel}$,

$$\langle G^{+}_{\vec{k}_\parallel,\vec{k}'_\parallel}\rangle = \frac{1}{(G^{+(0)}_{\vec{k}_\parallel})^{-1} - \Sigma}\delta_{\vec{k}_\parallel,\vec{k}'_\parallel}. \tag{41}$$

Now we see from Eqs. (29), (39), and (41) that by neglecting vertex corrections, the transmission probability is diagonal. This gives rise to specular scattering only. The diffuse part of the scattering comes exclusively from vertex corrections.

In the Born approximation the lowest two terms in the series of the irreducible self-energy are included; that is, first and second order scattering by an impurity (Fig. 10). This approximation is valid for low impurity densities $n_{IR} = N_{IR}/A$ and weak-scattering strength. Phase coherent scattering between different impurities can be shown to contribute only to order $O(n_{IR}^2)$ and is disregarded here. By using the Feynman rules for the diagrams, the self-energy in the Born approximation is given by the equation

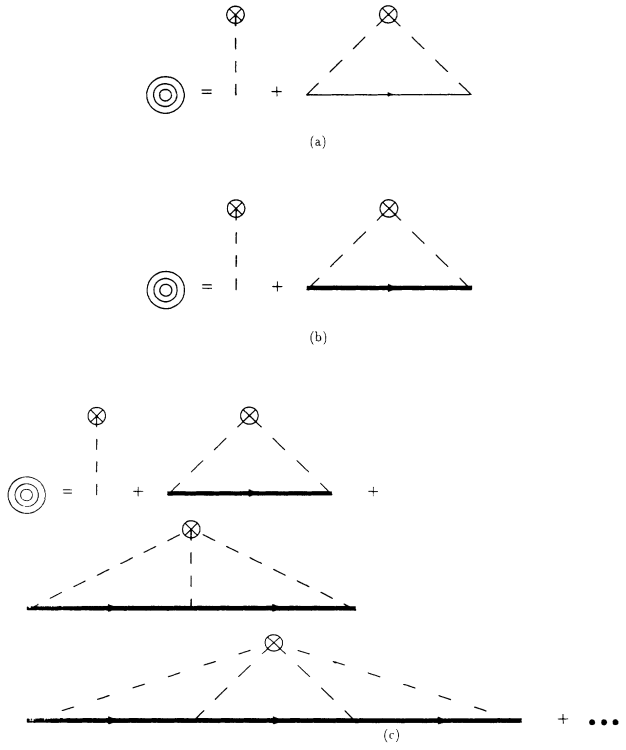

FIG. 10. The self-energy in (a) the Born approximation, (b) the self-consistent Born approximation, and (c) the single-site approximation.

$$\Sigma^B = \sum_\alpha \frac{\gamma_\alpha}{A} + \sum_\alpha (\frac{\gamma_\alpha}{A})^2 \sum_{\vec{k}_\parallel} G^{+(0)}_{\vec{k}_\parallel} \tag{42}$$

$$= n_{IR}\bar{\gamma} + n_{IR}\frac{\gamma^2}{A}\sum_{\vec{k}_\parallel} G^{+(0)}_{\vec{k}_\parallel}. \tag{43}$$

The average strength of the scatterers is $\bar{\gamma} = \sum_\alpha \gamma_\alpha/N$ and the mean square value is $\gamma^2 = \sum_\alpha \gamma_\alpha^2/N$. By neglecting the effect of the conduction-band step and effective-mass mismatch in the intermediate wave-vector summation over the unperturbed Green function, we find that (see Appendix C)

$$\Sigma^B = n_{IR}\bar{\gamma} - i\frac{m^*}{\hbar^2}\frac{n_{IR}}{2\pi}\gamma^2 k_F[1 - i\sqrt{\alpha^2 - 1}]. \tag{44}$$

Here, an ultraviolet divergence in the summation over intermediate evanescent states has been cut off at a wave vector αk_F to account for the finite range of the potential. $\alpha \geq 1$, but not much larger than unity, since the range cannot be shorter than a d orbital radius. We will show that the evanescent states are not important in the low-density/weak-scattering limit. The Born approximation is valid when $n_{IR}(m^*\gamma/\hbar^2)^2 \ll 1$.

More diagrams can be included in the self-energy if the unperturbed single propagator in the Born approximation is substituted by the renormalized one. This is the self-consistent Born approximation.[28] The diagrams are shown in Fig. 10. The self-consistent equation to solve is

$$\Sigma^{SB} = n_{IR}\bar{\gamma} + n_{IR}\frac{\gamma^2}{A}\sum_{\vec{k}_\parallel}\frac{1}{(G^{+(0)}_{\vec{k}_\parallel})^{-1} - \Sigma^{SB}}. \tag{45}$$

The self-energy appears on both sides of the equation, and therefore cannot become infinitely large. In the low-density/weak-scattering limit the self-consistent Born approximation reduces to the Born approximation, $\Sigma^{\mathrm{SB}} \approx \Sigma^B$. In the strong scattering limit, $n_{IR}(m^*\gamma/\hbar^2)^2 \gg 1$, the self-energy in the self-consistent Born approximation is

$$\Sigma^{\mathrm{SB}} = \frac{n_{IR}\bar{\gamma} - \sqrt{(n_{IR}\bar{\gamma})^2 - n_{IR}\gamma^2\frac{\alpha^2 k_F^2}{\pi}}}{2}. \tag{46}$$

In the zero average scatterer case ($\bar{\gamma} = 0$), this reduces to

$$\Sigma^{\mathrm{SB}} = -i\frac{\alpha k_F}{2}\sqrt{\frac{n_{IR}}{\pi}\gamma^2}. \tag{47}$$

The cutoff factor now plays an important role in determining the self-energy. This is reasonable since, as the scattering strength increases, the evanescent states become more important; a localized mode may build up at the interface.

We will now study the situation where all scatterers have equal strength, $\gamma_\alpha = \pm\gamma$. The self-energy is calculated in the so-called single-site approximation where the exact cross section for isolated defects is taken into account (Fig. 10). As mentioned above, crossed diagrams that stand for quantum interference between different defects are disregarded, which is allowed for small n_{IR}. The irreducible self-energy can be written as a geometric series which is summed to be

$$\Sigma^S = \frac{n_{IR}\bar{\gamma} + n_{IR}\frac{\gamma^2}{A}\sum_{\vec{k}_\parallel}\langle G^+_{\vec{k}_\parallel}\rangle}{1 - (\frac{\gamma}{A}\sum_{\vec{k}_\parallel}\langle G^+_{\vec{k}_\parallel}\rangle)^2}. \tag{48}$$

Consider now the case when the self-energy is small, $|(m^*/\hbar^2 k_F)\Sigma| \ll 1$. If the effect of the conduction-band step is neglected in the intermediate wave-vector summation, the self-energy becomes

$$\Sigma^S = \frac{n_{IR}\bar{\gamma} - in_{IR}\frac{m^*}{\hbar^2}\gamma^2\frac{k_F}{2\pi}(1 - i\sqrt{\alpha^2 - 1})}{1 + \left(\frac{m^*\gamma}{\hbar^2}\frac{k_F}{2\pi}\right)^2(1 - i\sqrt{\alpha^2 - 1})^2}. \tag{49}$$

In the weak-scattering limit, $m^*\gamma k_F/(\pi\hbar^2) \ll 1$; this result reduces to the result from the Born approximation. If the scattering strength is sufficiently strong, but the density of impurities low, the self-energy is

$$\Sigma^S = -in_{IR}\frac{\hbar^2}{m^*}\frac{2\pi}{k_F}\frac{1 + i\sqrt{\alpha^2 - 1}}{\alpha^2}. \tag{50}$$

In this strong-scattering limit, not the scattering strength but the spatial extent ($\propto 1/\alpha$) of the potential becomes the important parameter. The self-energy now vanishes for zero-range potentials, as it should. We will show that Eq. (50) has interesting consequences for the conductance.

Using the self-energies, we may now find the electron Green function in different approximations. In order to find the transmission probabilities, the vertex corrections also have to be found. This is done in the next subsection, where we will use a semiclassical approximation consistent with the single-site approximation for the self-energy.

B. Semiclassical approximation

In a semiclassical approximation, the optical theorem may be used to find a simple relation between the self-energy and the vertex function. The self-energy is only a constant, which represents a major simplification. The optical theorem, Eq. (31), can be written in terms of the unperturbed Green function, the irreducible self-energy, and the reducible vertex function,

$$\sum_{\vec{k}_\parallel}^{|\vec{k}_\parallel| \leq k^L_{\parallel,\max}} \frac{G^{+(0)*}_{\vec{k}_\parallel}}{|1 - G^{+(0)}_{\vec{k}_\parallel}\Sigma|^2} W_{\vec{k}_\parallel,\vec{k}'_\parallel} + \frac{1}{2}\sum_{|\vec{k}_\parallel| \geq k^L_{\parallel,\max}}^{|\vec{k}_\parallel| \leq k^R_{\parallel,\max}} \frac{k^R_\perp}{k_\perp}\frac{G^{+(0)*}_{\vec{k}_\parallel}}{|1 - G^{+(0)}_{\vec{k}_\parallel}\Sigma|^2} W_{\vec{k}_\parallel,\vec{k}'_\parallel} = -i\mathrm{Im}\Sigma, \tag{51}$$

by using Eqs. (39) and (41). This is actually a relation between the reducible vertex function and the irreducible

self-energy. In quantum field theory similar relations are referred to as Ward identities,[27] which are often employed as tests of the consistency of approximate theories. In the presence of disorder it is never consistent to neglect the vertex function in perpendicular transport, except for the ballistic regime where the self-energy vanishes.[29]

The reducible vertex function can be found directly using the irreducible vertex function from the Bethe-Salpeter integral equation, Eq. (40). The diagrams contributing to the irreducible vertex function can be classified as crossing or noncrossing. The crossing diagrams describe phase coherence and are, e.g., responsible for weak (Anderson) localization of the wave function.[30–32] In the generalized ladder approximation all crossing diagrams are disregarded in the calculation of the irreducible vertex function. Since the crossed terms contribute only to higher order in the impurity density, this is strictly allowed for sufficiently small n_{IR} . The "diamond" is considered as the irreducible vertex function as shown in Fig. 11, and is calculated in Appendix A. An important feature of this diamond is its independence of the outgoing and incoming state labels. The irreducible and the reducible vertex functions are therefore independent of the indices for noncrossing diagrams. Therefore, by neglecting crossing diagrams, i.e., phase coherent scattering between different impurities, Eq. (51) is easily inverted to give the reducible vertex function in terms of the irreducible self-energy,

$$W = \frac{-i\mathrm{Im}\Sigma}{\sum_{\vec{k}_\parallel}^{|\vec{k}_\parallel|\le k^L_{\parallel,\max}} \frac{G^{+(0)*}_{\vec{k}_\parallel}}{|1-G^{+(0)}_{\vec{k}_\parallel}\Sigma|^2} + \frac{1}{2}\sum_{|\vec{k}_\parallel|\ge k^L_{\parallel,\max}}^{|\vec{k}_\parallel|\le k^R_{\parallel,\max}} \frac{k^R_\perp}{\bar{k}_\perp} \frac{G^{+(0)*}_{\vec{k}_\parallel}}{|1-G^{+(0)}_{\vec{k}_\parallel}\Sigma|^2}}. \tag{52}$$

By calculating the self-energy in a given semiclassical approximation, we obtain the reducible vertex function, and the two-particle Green function without additional effort. By using the relation between the Green function and the transmission coefficient Eq. (29) and inserting Eq. (52) into Eq. (39), we find that the transmission probability is

$$\langle |t_{\vec{k}_\parallel,\vec{k}'_\parallel}|^2\rangle = \delta_{\vec{k}_\parallel,\vec{k}'_\parallel} \frac{k^R_\perp k^L_\perp}{|\bar{k}_\perp + i\frac{m^*}{\hbar^2}\Sigma|^2} + \frac{k^R_\perp}{|\bar{k}_\perp + i\frac{m^*}{\hbar^2}\Sigma|^2}\left[\left(\frac{m^*}{\hbar^2}\right)^2 (W)\right]\frac{k'^L_\perp}{|\bar{k}'_\perp + i\frac{m^*}{\hbar^2}\Sigma|^2}. \tag{53}$$

The self-energy determines both the specular and diffuse parts of the scattering. In specular scattering the transverse wave vector is conserved, which is the first term of Eq. (53). Diffuse scattering causes a redistribution of transverse and longitudinal momenta at the interface, which is the second term in Eq. (53). The ladder approximation and this consistency argument must give the same result, which is demonstrated explicitly in Appendix A for the weak-scattering limit. Diffuse and specular scattering are equally important in the weak-scattering limit. For strong scattering, the diffuse term dominates. Equation (53) completes our treatment of the single interface. It can be calculated readily for arbitrary model parameters.

Since for transition metal heterostructures $\Delta U_C/E_F \ll 1$ (for Co/Cu $\Delta U_C/E_F = 0.07$, Ref. 20), it appears a reasonable assumption to set $\Delta U_C = 0$ (but $\gamma_\alpha \neq 0$). Furthermore, we put $\Delta m = 0$, which is approximately true for the s bands in transition metals. These assumptions make an exact analytical treatment possible. It is interesting to make contact with the traditional treatment of interface roughness in terms of a specularity factor p. Let us introduce a specularity factor for *transmitted* electrons defined by

$$p_t(\theta) \equiv \frac{\langle T_{\vec{k}'_\parallel,\vec{k}'_\parallel}\rangle}{\sum_{\vec{k}_\parallel}^{\mathrm{prop}}\langle T_{\vec{k}_\parallel,\vec{k}'_\parallel}\rangle}, \tag{54}$$

which is found to be

$$p_t(\theta) = \frac{\cos(\theta)}{\eta_{IR} + \cos(\theta)}, \tag{55}$$

where $\eta_{IR} = -m^*\mathrm{Im}(\Sigma)/\hbar^2 k_F$ is a scattering parameter and θ is the angle of incidence of an electron wave vector measured from the surface normal. This result is valid in both the 2D and 3D cases. Note that the scattering parameter is independent of the real part of the self-energy. From Eq. (43) it is seen that the specularity parameter for transmission does not depend on the average of scatters, i.e., $\bar{\gamma}$. A similar relation can be derived for the ratio of specularly reflected electrons. It is found that $p_r(\theta) + p_t(\theta) = 1$ in the semiclassical approximation. In Fig. 12, the specularity factor p_t is shown as a function of the angle of incidence for $\eta_{IR} = 0.05$ and $\eta_{IR} = 0.5$. Diffuse scattering increases for larger incoming angles and for increasing values of the scattering parameter η_{IR}. Note, however, that the transmission probability itself vanishes when $\theta \to \pi/2$.

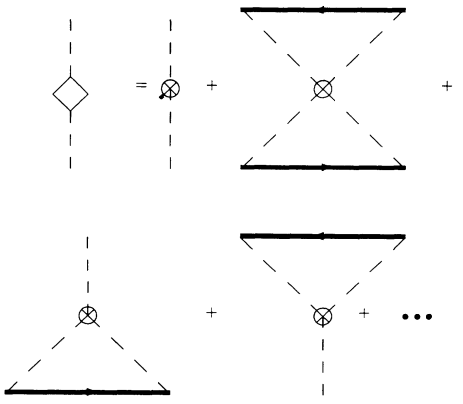

FIG. 11. All noncrossing diagrams in the irreducible vertex function give the diamond term.

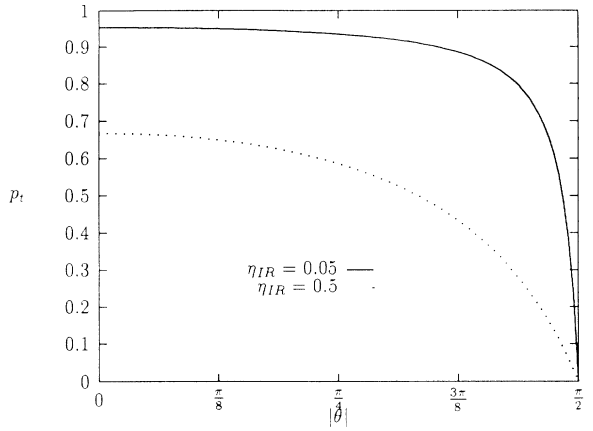

FIG. 12. Fraction of electrons transmitted specularly as a function of incoming angle to the relative interface normal.

Let us consider now the limit $|m^*\Sigma/\hbar^2| \ll k_F$, and use the single-site approximation for the self-energy Eq. (49). The transmission probability is then

$$\langle T_{\vec{k}_\parallel,\vec{k}'_\parallel}\rangle = \frac{(k_\perp)^2}{(k_\perp+\eta_{IR}k_F)^2}\delta_{\vec{k}_\parallel,\vec{k}'_\parallel} + \frac{k_\perp}{(k_\perp+\eta_{IR}k_F)^2}\frac{\eta_{IR}k_F}{\sum_{\vec{k}''_\parallel}\frac{k''_\perp}{(k''_\perp+\eta_{IR}k_F)^2}} \times \frac{k'_\perp}{(k'_\perp+\eta_{IR}k_F)^2}. \quad (56)$$

The contribution from the real part of the self-energy is not important in this limit. In the Born approximation $\{[(m^*\gamma k_F/(\hbar^2\pi)]^2 \ll 1\}$ the scattering parameter is $\eta_{IR} \approx (n_{IR}/(2\pi))(m^*\gamma/\hbar^2)^2$. When the Born approximation holds, evanescent modes are not important, but they play a significant role in the strong-scattering limit $\{[m^*\gamma k_F/(\hbar^2\pi)]^2 \gg 1\}$.

The conductance can now be found by inserting the transmission probability, Eq. (56), into the Landauer-Büttiker formula, Eq. (1). To first order in the scattering parameter η_{IR}, the conductance is

$$G = \frac{2e^2}{h}\frac{Ak_F^2}{4\pi}[1-4\eta_{IR}+2\eta_{IR}]. \quad (57)$$

The first term is the Sharvin conductance,[19] which is proportional to the sample cross section A. The second term reduces the conductance due to specular scattering. The third, diffusive term *increases* the conductance by opening additional channels for electron transport. In the single-site approximation for strong scattering $[(m^*\gamma k_F/\hbar^2\pi)^2 \gg 1]$, but to lowest order in η_{IR}, we obtain the interesting result that

$$G = \frac{2e^2}{h}\left(\frac{Ak_F^2}{4\pi} - \frac{N_{IR}}{\alpha^2}\right). \quad (58)$$

The conductance is reduced by a factor proportional to the number of defects $N_{IR} = An_{IR}$, which can be also derived from a direct solution of the Schrödinger equation (see Appendix B). Each scatterer effectively blocks one channel and the conductance becomes independent of the scattering strength. This blocking is somewhat reduced by a factor $1/\alpha^2$ via a "leak" of evanescent states. Alternatively, we can interpret the second term as a finite size effect; the conductance is reduced by a term proportional to the finite spatial cross section of the scatterers. An experiment is proposed to check this expression: Insert a layer (or multilayer, see the next section) with strong short-range scatterers between two perfect leads. Such a structure could be realized by the technique of δ doping, which is routinely employed in semiconductor technology. By measuring the conductance and the number of impurities the theory can be checked and the "leaking factor" α determined, which provides information about the scattering potential. Note that a nonzero average of scatterers has negligible effect on the conductance. A similar result is valid in the 2D electron gas case, with a leaking factor as a function of α.

V. GENERALIZATION TO A MULTILAYER

In the preceding section the scattering properties of a single interface have been investigated. In the present section we will show that we can get semiclassical results for a system of N interfaces, and that bulk impurity scattering can be consistently taken into account. Results for a single interface can be generalized to a multilayer situation with interface and bulk impurity scattering. In principle it is possible to find the transmission coefficient for two or more interfaces if the transmission coefficient for one interface is known, but the calculation is very cumbersome in general. The interferences due to multiple reflections at the interface potential steps can be disregarded if $(\Delta U/E_F \ll 1)$ which is the case for s electrons in transition metal systems, or if the phase-coherence length or mean free path are smaller than the layer widths. Interfering multiple reflections at defects on different interfaces are also suppressed by phase breaking scattering, but can be also disregarded for small defect densities. Semiclassical concatenation[21] is consistent with the single-site approximation for single interface scattering. In order to get an exact concatenation of the transmission coefficient, the ensemble average has to be taken after the concatenation, which seems to make an analytical treatment complicated, even in a semiclassical approximation. We will show here that the problem is greatly simplified by using the optical theorem.

Consider two scattering events where $\bar{\bar{T}}_1$ ($\bar{\bar{R}}_1$) is the transmission (reflection) probability for the first interface, and $\bar{\bar{T}}_2$ ($\bar{\bar{R}}_2$) is the transmission (reflection) probability for the second interface for propagation from left to right. Similarly, a prime on the matrices will denote propagation from right to left. Semiclassically, two scattering events can be concatenated as[21]

$$\bar{\bar{T}}_{12} = \bar{\bar{T}}_2[\bar{\bar{I}} - \bar{\bar{R}}'_1\bar{\bar{R}}_2]^{-1}\bar{\bar{T}}_1 \quad (59)$$

and

$$\bar{\bar{R}}_{12} = \bar{\bar{R}}_1 + \bar{\bar{T}}'_1\bar{\bar{R}}_2[\bar{\bar{I}} - \bar{\bar{R}}'_1\bar{\bar{R}}_2]\bar{\bar{T}}_1, \quad (60)$$

where $\bar{\bar{T}}_{12}$ ($\bar{\bar{R}}_{12}$) is the transmission (reflection) probability for transport from left to right through the whole system. This is easily seen as a geometric series of multiple reflections between the two interfaces. For simplicity, only the symmetric case will be considered in the following, i.e., $\Delta U_C/E_F \ll 1$ and $|(m_R^*-m_L^*)/(m_R^*+m_L^*)| \ll 1$. The scattering at the interface due to interface roughness is taken into account, but the effect of a finite $\Delta U_C/E_F$ on the transmission probability is disregarded.

Let us now consider the simple case where the transmission probability is diagonal,

$$T_{12} = \frac{T_1}{2-T_1}. \tag{61}$$

The transmission probability for transport through N interfaces is

$$T^{(N)} = \frac{T_1}{N-(N-1)T_1}, \tag{62}$$

which may be verified by induction from Eqs. (59) and (60). For the general nondiagonal case we have not been able to find such a simple relation.

Semiclassical concatenation of the diagonal part of the transmission probability, Eq. (56), gives

$$\langle T^{(N)\mathrm{spec}}_{\vec{k}_\parallel,\vec{k}'_\parallel}\rangle = \delta_{\vec{k}_\parallel,\vec{k}'_\parallel}\frac{k_\perp}{k_\perp + 2N\eta_{IR}k_F} \tag{63}$$

in the small η_{IR} regime. Here only the specular part of the scattering is included, which is not consistent with the Ward identity as stated in the preceding section. However, the result for the N-layer specular case will form an important reference frame. Inserting the transmission probabilities, Eq. (63), into the Landauer-Büttiker formula, Eq. (1), we find that the conductance is

$$\frac{G^{(N)\mathrm{spec}}}{G_0} = 1 - 2(2N\eta_{IR}) + 2(2N\eta_{IR})^2\ln(1+\frac{1}{2N\eta_{IR}}), \tag{64}$$

when only specular scattering is taken into account. We will now include contributions from diffuse scattering to the conductance.

The transmission properties do not depend on the distance between the interfaces in a semiclassical approximation. By allowing the interfaces to be infinitesimally close to each other, one can convince oneself that the relation between the transmission probabilities and the transmission coefficients, Eq. (22), still holds for the N-interfaces configuration,

$$\sum_{\vec{k}_\parallel} T_{\vec{k}_\parallel,\vec{k}'_\parallel} = \mathrm{Re}(t_{\vec{k}'_\parallel,\vec{k}'_\parallel}). \tag{65}$$

The diagonal transmission coefficient is given by the electron Green function, i.e., the specular part of the scattering. From Eq. (56) we find that the transmission coefficient is

$$\langle t_{\vec{k}_\parallel,\vec{k}'_\parallel}\rangle = \frac{k_\perp}{k_\perp + \eta_{IR}k_F}\delta_{\vec{k}_\parallel,\vec{k}'_\parallel} \tag{66}$$

in the weak-scattering limit. It is important that the weak-scattering limit be taken before concatenation. Otherwise all defects placed at the same interface would be incorrectly equivalent to a single strong-scattering interface. Concatenation of the *diagonal* transmission coefficients, Eq. (66), is straightforward. By using Eq. (65) after the concatenation, the conductance for transport through N interfaces is

$$\frac{G^{(N)}}{G_0} = 1 - 2(N\eta_{IR}) + 2(N\eta_{IR})^2\ln\left[1+\frac{1}{N\eta_{IR}}\right]. \tag{67}$$

The scattering parameter is decreased by a factor of 2 compared to the purely specular case.

The results for N interfaces can be generalized to treat the bulk system. A bulk system is modeled by N interfaces with an interface scattering parameter $\eta_{BI}^{2\mathrm{D}}$. The conductance for the bulk system may be found by letting $N\to\infty$ and $\eta_{BI}^{2\mathrm{D}}\to 0$, but keeping $N\eta_{BI}^{2\mathrm{D}} = L\eta_{BI}$, where L is the length of the bulk material and, η_{BI} is the scattering parameter for the bulk system. The conductance for a multilayer is

$$\frac{G^{(N)}}{G_0} = 1 - 2x_N + 2x_N^2\ln\left[1+\frac{1}{x_N}\right], \tag{68}$$

where $x_N = N/(2\bar{N}) = L/(2l)$, $\bar{N}$ is the mean free number of traversed interfaces given by $\bar{N} \equiv [2\eta_{IR} + 2L\eta_{BI}]^{-1}$, and l is the mean free path. This relation agrees with Eq. (11) in Ref. 7 for $\Delta U_C = 0$. The results are easily generalized to arbitrary impurity distributions, which represent, e.g., interdiffused interfaces. The semiclassical expression for the self-energy Σ_{tot} (or the scattering parameter η_{tot}) for the whole sample reads

$$\Sigma_{\mathrm{tot}} = N\Sigma_{IR} + \int dx\Sigma_{BI}(x), \tag{69}$$

where $\Sigma_{BI}(x)$ is the position dependent self-energy determined by the local impurity density and scattering strength. For a small number of layers, the conductance decreases in proportion to the ratio of the number of layers to the mean free number of traversed layers. In the large N limit a Drude-like (Ohm's law) expression is obtained for the conductivity of a thick multilayer

$$\sigma_\infty = \lim_{N\to\infty} NLG^{(N)}\Big/A = \frac{2e^2}{h}\frac{k_F^2}{3\pi}l, \tag{70}$$

which agrees with the results of Zhang and Levy.[6,33] The conductivity is proportional to the mean free number of traversed interfaces. The conductance of a nonmagnetic multilayer is plotted in Fig. 13. The Drude result is approached rather slowly.[7]

The two-dimensional equivalent of this expression is of interest in quasiballistic transport in semiconductor nanostructures[34,35]

$$\frac{G_{2D}^{(N)}}{G_{2D}^{0}} = 1 - \frac{x_N \pi}{2} + \begin{cases} \frac{x_N^2}{\sqrt{1-x_N^2}} \ln\left(\frac{1+\sqrt{1-x_N^2}}{x_N}\right), & x_N < 1 \\ \frac{x_N^2}{\sqrt{x_N^2-1}} \arccos\left(\frac{1}{x_N}\right), & x_N > 1, \end{cases} \tag{71}$$

where $G_{2D}^{0} = (2e^2/h)(Wk_F/\pi)$ is the two-dimensional Sharvin conductance, proportional to the channel width. In the Drude limit, we find

$$\sigma_\infty = \lim_{N\to\infty} \frac{NL_p G_{2D}^{N}}{W} = \frac{2e^2}{h}\frac{k_F}{2} l. \tag{72}$$

De Jong solved the Boltzmann equation to obtain results which are very similar, but not identical to the expressions Eqs. (68) and (71).[35] We must therefore conclude that the present semiclassical approximation is not equivalent to the solution of the Boltzmann equation. One of the qualitative differences is the back reflection of grazing incidence electrons in the present approach, which are transmitted with finite probability in the Boltzmann approach.[35] The reason is the wave character of electron states even in our semiclassical approximation.

The effect of the conduction-band step on the conductance can be found by concatenation of Eq. (53), for which Eq. (12) in Ref. 7 is only an approximation. This has to be done numerically, since the expression for the N-layer conductance is very complicated. In our model the quantum interference effects between the interfaces are neglected. The calculation based on a tight-binding model by Asano, Oguri, and Maekawa,[10] however, suggests that the semiclassical approximation breaks down when the step height is sufficiently large. We therefore refrain from carrying out the computation here.

For a magnetic multilayer it is now straightforward to find the conductance by including spin-dependent interface scattering and bulk scattering. Let $\bar{N}_{maj}$ ($\bar{N}_{min}$) be the mean free number of traversed interfaces for the majority (minority) spins in the parallel configuration. The difference in mean free path between both spin channels is $\Delta\bar{N}$ and the spin-averaged number is $\bar{N}$. The conductance for the parallel configuration, G^P, and the conductance for the antiparallel configuration, G^{AP} are straightforward generalizations of Eq. (68). In Fig. 14 the relative magnetoconductance of the antiparallel configuration $\Delta G/G^P$ is shown, where $\Delta G = G^P - G^{AP}$. The relative magnetoconductance depends on the ratios $\Delta\bar{N}/\bar{N}$ and $N_{bi}/\bar{N}$, where N_{bi} is the number of bilayers. In the present approximation each layer contributes independently to the CPP magnetoresistance and the results do not require an ordered antiparallel alignment as long as the number of up and down spin interfaces remains the same. The spin valve saturates at the Drude limit for $N_{bi} \gg \bar{N}$. In this superlattice limit the relative magnetoconductance is

$$\left(\frac{\Delta G}{G^P}\right)^{Drude} = \left(\frac{1}{2}\frac{\Delta\bar{N}}{\bar{N}}\right)^2. \tag{73}$$

For $\Delta\bar{N} = 0$ the magnetoconductance vanishes, and it becomes unity for $\Delta\bar{N} = 2\bar{N}$ (i.e., the minority-spin channel is totally blocked, $\bar{N}_{min} = 0$). The spin filter improves with increasing thickness by the scattering from imperfections.

VI. CONCLUSIONS

We have derived expressions for semiclassical perpendicular transport in metallic multilayers, which are exact for the present model. An experiment to check the theory is proposed, which might lead to a deeper understanding of the scattering process and the microscopic structure of disordered interfaces. The transition from ballistic to diffuse transport in 2D and 3D systems is given by an exact analytical expression (within our semiclassical approximation). A simple semiclassical formula for the giant magnetoconductance of antiparallel coupled magnetic multilayers in terms of the mean free number

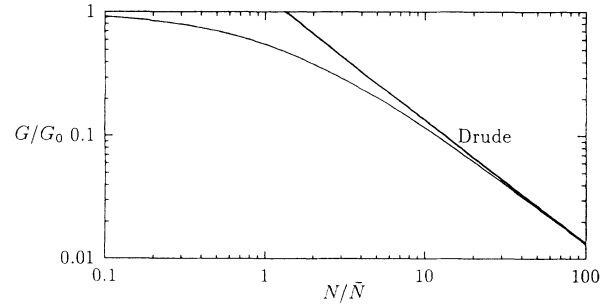

FIG. 13. Conductance of a spinless multilayer as a function of the number of layers N relative to the mean free number $\bar{N}$. The dashed line is the Drude result.

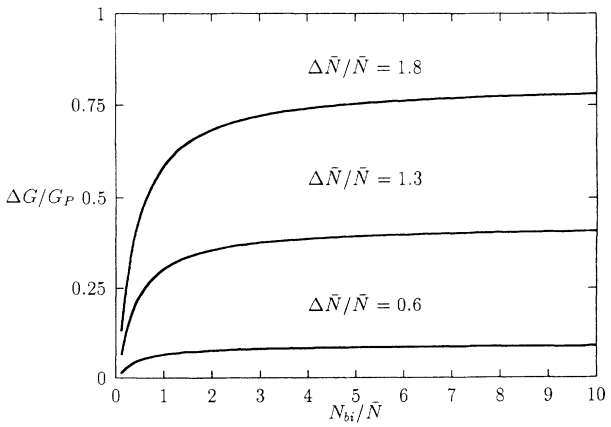

FIG. 14. Magnetoconductance for an antiparallel coupled magnetic multilayer. The solid curves illustrate the effect of spin-dependent mean free number of traversed interfaces.

of traversed interfaces (or mean free path) for majority and minority spins is derived. The parameters of the theory are as yet phenomenological, but the formalism can be extended to include the CIP geometry,[36] spin-flip scattering,[36] quantum interference including realistic band structure effects,[17,37] and more realistic models of impurity and interface roughness scattering.

ACKNOWLEDGMENTS

We thank Alexander Khaetskii, Marc de Jong, Kees Schep, John Ove Fjærestad, and Martin Gijs for helpful discussions. This work is part of the research program of the "Stichting voor Fundamenteel Onderzoek der Materie (FOM)," which is financially supported by the "Nederlandse Organisatie voor Wetenschappenlijk Onderzoek (NWO)."

APPENDIX A: GENERALIZED LADDER APPROXIMATION

In this appendix we will calculate the total vertex function directly from the irreducible vertex function in the generalized ladder approximation. In a semiclassical approximation, the phase coherence between scattering at different impurities described by crossing diagrams is neglected. The irreducible vertex function is the diamond term in Fig. 11,

$$\sigma_{\vec{k}_\parallel,\vec{k}'_\parallel}=\sum_\alpha\left\{\left(\frac{\gamma_\alpha}{A}\right)^2\sum_{N=0}^{\infty}\left(\frac{\gamma_\alpha}{A}\sum_{\vec{k}''_\parallel}\langle G^+_{\vec{k}''_\parallel}\rangle\right)^N\sum_{M=0}^{\infty}\left(\frac{\gamma_\alpha}{A}\sum_{\vec{k}'''_\parallel}\langle G^{+*}_{\vec{k}'''_\parallel}\rangle\right)^M\right\}, \tag{A1}$$

by using the Feynman rules from Sec. III C. It is seen that the irreducible vertex function is independent of the wave vectors of outgoing and incoming states, $\sigma_{\vec{k}_\parallel,\vec{k}'_\parallel}=\sigma$. This simplifies the calculation considerably. It is the basis for the semiclassical approximation in Sec. IV B, where the reducible vertex function is found in terms of the self-energy. Here we choose a different approach and calculate the reducible vertex function directly from the irreducible vertex function.

The reducible vertex function is related to the irreducible vertex function by the Bethe-Salpeter integral equation,

$$W_{\vec{k}_\parallel,\vec{k}'_\parallel}=\sigma_{\vec{k}_\parallel,\vec{k}'_\parallel}+\sum_{\vec{k}''_\parallel}\sigma_{\vec{k}_\parallel,\vec{k}''_\parallel}|\langle G^+_{\vec{k}''_\parallel}\rangle|^2W_{\vec{k}''_\parallel,\vec{k}'_\parallel}. \tag{A2}$$

Just like the irreducible vertex function, the reducible one does not depend on the indices. The Bethe-Salpeter integral equation is then easily solved,

$$W=\frac{\sigma}{1-\sigma\sum_{\vec{k}_\parallel}|\langle G^+_{\vec{k}_\parallel}\rangle|^2}. \tag{A3}$$

Let us consider the low-density, weak-scattering limit. In this limit the reducible vertex function and the irreducible vertex function are equal. To the lowest order in γ we see from Eq. (A1) that the reducible vertex function is simply

$$W=n_{IR}\gamma^2/A. \tag{A4}$$

The self-energy is calculated in the Born approximation, Eq. (43). By inserting Eq. (A4) into the expression for the two-particle Green function, Eq. (39), and using the relation between the Green function and the transmission coefficient, Eq. (29), we find that the transmission probability is

$$\langle T_{\vec{k}_\parallel,\vec{k}'_\parallel}\rangle=\frac{k_\perp^2}{(k_\perp+\eta_{IR})^2}\delta_{\vec{k}_\parallel,\vec{k}_\parallel}+\frac{k_\perp}{(k_\perp+\eta_{IR})^2}\frac{2\pi\eta_{IR}}{A}\frac{k'_\perp}{(k'_\perp+\eta_{IR})^2} \tag{A5}$$

in this approximation. Here $\eta_{IR}=[n_{IR}/(2\pi)](m^*\gamma/\hbar^2)^2$. This result agrees with the transmission probability found from the Ward identity, Eq. (56), in the Born approximation.

APPENDIX B: SINGLE SHORT-RANGE SCATTERER

In this appendix we consider scattering from a single scatterer in the channel. The scattering matrix as defined in Eq. (15) is, for a single scatterer located at $\vec{\rho}_\alpha=0$ with scattering strength γ,

$$\tilde{\Gamma}_{\vec{k}_\parallel,\vec{k}'_\parallel}=\frac{m^*\gamma}{\hbar^2}\frac{1}{L^{d-1}}, \tag{B1}$$

where d is the dimension of the channel. The matrix equation to solve is given in Eq. (24):

$$\sum_{\vec{k}''_\parallel}[\delta_{\vec{k}_\parallel,\vec{k}''_\parallel}+i\tilde{\Gamma}_{\vec{k}_\parallel,\vec{k}''_\parallel}\sqrt{\frac{|k_\perp^R|}{|k''^R_\perp|}}\frac{1}{2\bar{k}_\perp}]t_{\vec{k}''_\parallel,\vec{k}'_\parallel}=\frac{\sqrt{|k_\perp^L||k_\perp^R|}}{\bar{k}_\perp}\delta_{\vec{k}_\parallel,\vec{k}'_\parallel}. \tag{B2}$$

In the symmetric case ($k_\perp^L=k_\perp^R$) this equation may be written as

$$t_{\vec{k}_\parallel,\vec{k}_\parallel}+i\sqrt{\Gamma_{\vec{k}_\parallel}}\frac{|k_\perp|}{k_\perp}\sum_{\vec{k}''_\parallel}\sqrt{\Gamma_{\vec{k}''_\parallel}}t_{\vec{k}''_\parallel,\vec{k}_\parallel}=\delta_{\vec{k}_\parallel,\vec{k}'_\parallel}, \tag{B3}$$

where

$$\Gamma_{\vec{k}_\parallel} \equiv \frac{m^*\gamma}{2\hbar^2 L^{d-1}|k_\perp|}. \tag{B4}$$

Solving this equation exactly, we find

$$t_{\vec{k}_\parallel,\vec{k}'_\parallel} = \delta_{\vec{k}_\parallel,\vec{k}'_\parallel} - i\sqrt{\Gamma_{\vec{k}_\parallel}}\frac{|k_\perp|}{k_\perp}\frac{\sqrt{\Gamma_{\vec{k}'_\parallel}}}{1+i\sum_{\vec{k}_\parallel}\Gamma_{\vec{k}_\parallel}}. \tag{B5}$$

By using the optical theorem, Eq. (22), the conductance in the limit of strong scattering ($\gamma \to \infty$) is found to be

$$G = \frac{2e^2}{h}\left[\sum_{\vec{k}_\parallel}^{\text{prop}}(1) - \frac{\left(\sum_{\vec{k}_\parallel}^{\text{prop}}\frac{1}{k_\perp}\right)^2}{\left(\sum_{\vec{k}_\parallel}^{\text{prop}}\frac{1}{k_\perp}\right)^2 + \left(\sum_{\vec{k}_\parallel}^{\text{evan}}\frac{1}{|k_\perp|}\right)^2}\right]. \tag{B6}$$

For a 3D channel, we find

$$G = \frac{2e^2}{h}\left(\frac{Ak_F^2}{4\pi} - \frac{1}{\alpha^2}\right), \tag{B7}$$

which is consistent with Eq. (58) for one single impurity. A similar result can be obtained for a 2D channel.

APPENDIX C: SUMMATION OF GREEN FUNCTIONS

The expression for the Dyson equation involves summations of the unperturbed Green functions which are carried out in this appendix. The effect of the discontinuities in the conduction-band profile and the effective mass in the intermediate wave-vector summation are disregarded. The electron Green function is given by the unperturbed Green function and the self-energy,

$$\langle G^+_{\vec{k}_\parallel}\rangle = \frac{1}{\left(-i\frac{m^*}{\hbar^2}\frac{1}{k_\perp}\right)^{-1} - \Sigma}. \tag{C1}$$

The summation over the electron Green function is

$$\sum_{\vec{k}_\parallel}\langle G^+_{\vec{k}_\parallel}\rangle = -i\frac{m^*}{\hbar^2}\sum_{\vec{k}_\parallel}\frac{1}{k_\perp + i\frac{m^*}{\hbar^2}\Sigma}, \tag{C2}$$

where $k_\perp = [k_F^2 - k_\parallel^2]^{1/2}$. Carrying out the integral,

$$\sum_{\vec{k}_\parallel}\langle G^+_{\vec{k}_\parallel}\rangle = -i\frac{m^*}{\hbar^2}\frac{Ak_F}{2\pi}\left\{1 - \frac{im^*\Sigma}{k_F\hbar^2}\ln\left(1+\frac{k_F}{i\frac{m^*}{\hbar^2}\Sigma}\right) - i\left[\sqrt{\alpha^2-1} - \frac{m^*\Sigma}{k_F\hbar^2} \times \ln\left(1+\frac{\sqrt{\alpha^2-1}k_F}{\frac{m^*}{\hbar^2}\Sigma}\right)\right]\right\}. \tag{C3}$$

Here an ultraviolet divergence in the summation over intermediate evanescent states has been cut off at a wave vector αk_F to account for the finite range of the potential. Similarly, the summation of the unperturbed Green function gives

$$\sum_{\vec{k}_\parallel} G^{+(0)}_{\vec{k}_\parallel} = -i\frac{m^*}{\hbar^2}\frac{Ak_F}{2\pi}[1 - i\sqrt{\alpha^2-1}]. \tag{C4}$$

These results are used in the calculation of the self-energy in Sec. IV A.

[1] P. Grünberg, R. Schreiber, Y. Pang, M. B. Brodsky, and C. H. Sowers, Phys. Rev. Lett. **57**, 2442 (1986).
[2] C. Kittel, *Quantum Theory of Solids* (John Wiley & Sons, New York, 1963).
[3] M. N. Baibich, J. M. Broto, A. Fert, F. Nguyen van Dau, and F. Petroff, Phys. Rev. Lett. **61**, 2472 (1988); G. Binasch, P. Grünberg, F. Saurenbach, and W. Zinn, Phys. Rev. B **39**, 4828 (1989). For a recent review see R. Coehoorn, Europhys. News **24**, 43 (1993).
[4] W. P. Pratt, S. F. Lee, R. Lolee, P. A. Schroeder, and J. Bass, Phys. Rev. Lett. **66**, 3060 (1991); W. P. Pratt *et al.*, J. Magn. Magn. Mater. **126**, 406 (1993).
[5] M. Gijs, S. K. J. Lenczowski, and J. B. Giesberg, Phys. Rev. Lett. **70**, 3343 (1993).
[6] S. Zhang, and P. M. Levy, J. Appl. Phys. **69**, 4786 (1991).
[7] G. E. W. Bauer, Phys. Rev. Lett. **69**, 1676 (1992).
[8] R. Q. Hood and L. M. Falicov, Phys. Rev. B **46**, 8287 (1992).
[9] T. Valet and A. Fert, Phys. Rev. B **48**, 7099 (1993).
[10] Y. Asano, A. Oguri, and S. Maekawa, Phys. Rev. B **48**, 6192 (1993).
[11] K. Fuchs, Proc. Philos. Camb. Soc. **34**, 100 (1938).
[12] T. Ando, A. B. Fowler, and F. Stern, Rev. Mod. Phys. **54**, 437 (1982).
[13] S. B. Soffer, J. Appl. Phys. **38**, 1710 (1967).
[14] R. Landauer, Z. Phys. B **68**, 217 (1987).
[15] A. Brataas and G. E. W. Bauer, Europhys. Lett. (to be published).
[16] A. Brataas and G. E. W. Bauer, Solid-State Electron. (to be published).
[17] G. E. W. Bauer, A. Brataas, C. M. Schep, and P. J. Kelly, J. Appl. Phys. (to be published).
[18] E. C. Stoner, Proc. R. Soc. London Ser. A **165**, 372 (1938).
[19] Y. V. Sharvin, Zh. Eksp. Teor. Fiz. **48**, 984 (1965) [Sov. Phys. JETP **21**, 655 (1965)].
[20] J. Inoue, A. Oguri, and S. Maekawa, J. Phys. Soc. Jpn. **60**, 376 (1990).
[21] B. Shapiro, Phys. Rev. B **35**, 8256 (1987); M. Cahay, M. McLennan, and S. Datta, *ibid.* **37**, 10 125 (1988).
[22] P. H. Bagwell, Phys. Rev. B **41**, 10 354 (1990).
[23] Y. B. Levinson, M. I. Lubin, and E. V. Sukhorukov, Phys. Rev. B **45**, 11 936 (1992).
[24] J. Kucera and P. Streda, J. Phys. C **21**, 4357 (1987).
[25] H. U. Baranger and A. D. Stone, Phys. Rev. B **40**, 8169 (1989).
[26] D. S. Fisher and P. A. Lee, Phys. Rev. B **23**, 6851 (1981).
[27] G. D. Mahan, *Many-Particle Physics*, 2nd ed. (Plenum Press, New York, 1990).

[28] T. Ando and Y. Uemura, J. Phys. Soc. Jpn. **36**, 959 (1974).
[29] In the case $\mathrm{Im}(\Sigma) \approx 0$, the vertex corrections vanish. This situation is possible for $\sum_\alpha \gamma_\alpha \neq 0$ and $\sum_\alpha \gamma_\alpha^2$ negligible, a situation not considered here.
[30] P. A. Lee and T. V. Ramakrishnan, Rev. Mod. Phys. **57**, 2 (1985).
[31] G. Bergmann, Phys. Rep. **107**, 1 (1984).
[32] P. W. Anderson, Phys. Rev. **109**, 1492 (1958).
[33] S. Zhang and P. M. Levy, Phys. Rev. B **45**, 8689 (1992).
[34] S. Tarucha, T. Saku, Y. Tokura, and Y. Hirayama, Phys. Rev. B **47**, 4064 (1993).
[35] M. J. M. de Jong, Phys. Rev. B (to be published); private communication.
[36] J. O. Fjærestad, A. Brataas, and G. E. W. Bauer (unpublished).
[37] C. M. Schep, P. J. Kelly, and G. E. W. Bauer (unpublished).

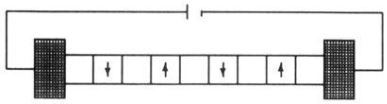

FIG. 1. A model of a magnetic multilayer structure.